Sulfur Poisoning of SOFC Anodes: Effect of Overpotential on Long-Term Degradation

Hauch, Anne; Hagen, Anke; Hjelm, Johan; Ramos, Tania

Published in:
Electrochemical Society. Journal

Link to article, DOI:
10.1149/2.080406jes

Publication date:
2014

Document Version
Publisher's PDF, also known as Version of record

Sulfur Poisoning of SOFC Anodes: Effect of Overpotential on Long-Term Degradation

A. Hauch,[z] A. Hagen, J. Hjelm,[*] and T. Ramos[*]

Department of Energy Conversion and Storage, Technical University of Denmark, Risø Campus, DK-4000 Roskilde, Denmark

Sulfur impurities in carbon containing fuels for solid oxide fuel cells (SOFC), e.g. natural gas and biogas, typically lead to significant losses in performance due to the sulfur sensitivity of Ni/yttria-stabilized-zirconia (YSZ) anodes for SOFC. Full cells having Ni/YSZ anodes have been characterized during long-term galvanostatic operation in internal reforming gas mixture ($CH_4/H_2O/H_2$:30/60/10), with 2 ppm H_2S exposure to the anode for 500 hours at 850°C, at different current densities. This work focus on the long-term effect of H_2S exposure over a few hundreds of hours; and describes and correlates the observed evolution of anode performance, over hundreds of hours, with sulfur exposure at low cell overpotential (low current density) and at high overpotential (high current density) with and without H_2S exposure. For tests at low overpotential with H_2S exposure only a reversible loss in performance was observed and post-mortem SEM analysis showed an intact Ni/YSZ anode microstructure. For tests at high cell overpotential the H_2S exposure caused both a reversible loss in performance and an irreversible long-term degradation. Post-mortem SEM analysis of the Ni/YSZ anode from this tests showed increased porosity and lack of percolating Ni in the few microns of the anode closest to the anode/electrolyte interface.

Manuscript submitted March 27, 2014; revised manuscript received April 25, 2014. Published May 6, 2014.

Fuel flexibility is an attractive characteristic of solid oxide fuel cells (SOFC). They can for instance be fuelled with carbon containing fuels such as natural gas or fuels derived from biomass. A well-known drawback for the use of carbon containing fuels is the fact that they contain varying amounts of sulfur, which poisons Ni-based SOFC anodes.[1–8] Therefore, it is important to investigate the SOFC tolerance toward sulfur poisoning and how it is affected by operating parameters.

There are many studies concerning the initial, and mainly reversible, loss in performance occurring at SOFC anodes upon sulfur poisoning as a function of different operating conditions.[4,7–9] Fewer results are reported on the long-term, and often irreversible, loss of performance due to sulfur poisoning,[5,8,10] even though this will inevitably be of high importance for SOFC as an emerging energy conversion technology. In order to establish the acceptable limits for sulfur impurities in carbon containing fuels in order to avoid long-term, irreversible degradation,[5,11] it is necessary to understand how the sulfur impurity tolerance correlate to operating parameters such as gas mixtures, temperature and current density, and indirectly to the cell overpotential.

It has been suggested that Ni-zirconia based SOFC anodes containing Sc are more tolerant toward H_2S poisoning than Ni/YSZ based anodes[5,7] and in this work both short and long term tests were performed to investigate this hypothesis. Tests were mainly carried out at the same set of test conditions (e.g. temperature, current density, fuel) in order to compare Sc-Y co-doped (ScYSZ) and Y doped zirconia (YSZ) Ni cermet SOFC anodes. There are several studies showing the effect of H_2S poisoning of Ni-YSZ based SOFC anodes as a function of parameters such as temperature, fuel gas composition and $p(H_2S)$ as summarized by Chen et al.[8] However, such parameters (temperature, current density, fuel utilization etc.) are all externally set parameters and they do not necessarily impose identical conditions internally in the electrodes of different cells e.g. in terms of electrode overpotentials and current distributions. This work is a study of the long-term H_2S poisoning effects on Ni-cermet SOFC anodes as a function of cell overpotential, rather than focusing on externally set parameters such as temperature, current density and gas compositions.

This work reports the results from long-term exposure to H_2S containing $CH_4/H_2O/H_2$ fuel mixtures at 850°C, with and without the presence of 2 ppm H_2S, for 500 h of galvanostatic testing at different cell overpotentials. The degradation behavior is investigated via cell voltage curves, detailed analyzes of electrochemical impedance spectra and post-mortem SEM analyzes – qualitative and quantitative – of the anodes from the different tests. Furthermore, correlations between the chosen cell overpotentials, measured long-term irreversible degradation behavior and resulting microstructural changes of the SOFC anodes are given.

Experimental

Cell specifications and test set-up.— The cells used for fuel cell testing in this study are anode supported full SOFC produced at the Department of Energy Conversion and Storage, Risø Campus, Technical University of Denmark.[12–15] The cells have a 10–15 μm thick anode of Ni/YSZ cermet with a ~300 μm thick Ni/YSZ support layer, a 10–15 μm thick YSZ electrolyte and a 15–20 μm thick LSM-YSZ composite cathode.[12] The ratio between Ni and YSZ is 40/60 by volume both for the support layer and the active electrode layer.[16] 8 mole percent Y_2O_3 stabilized zirconia (8YSZ) is used for the electrolyte and the active electrode layer. 3 mole percent Y_2O_3 stabilized zirconia is used for the support layer. The anode half cells (electrolyte, active anode and anode support layer) were produced via tape casting and lamination, followed by co-sintering of the half cell.[17] The cells have an anode support layer thickness of ~ 300 μm, an active anode layer thickness of 12 μm and porosities similar to those previously reported.[18] All cells reported in this study originate from the same tape of anode half-cell. The composition of the LSM is $(La_{0.75}Sr_{0.25})_{0.95}MnO_3$ and the ratio between LSM and YSZ in the composite electrode is LSM/YSZ = 50/50 by volume,[19] The LSM/YSZ cathode and LSM contact layer were applied via screen printing. For the cell for the H_2S free test, the LSM/YSZ cathode was substituted by a LSC/CGO based cathode and CGO barrier layer.[20] The higher performing LSC/CGO cathode was chosen to ensure that the cathode overpotential would not be dominating at the very high current density that was necessary to apply for the H_2S free test to reach anode overpotentials comparable with the H_2S tests. From the sintered anode half-cell tape cells sized 5 × 5 cm^2 are cut and 4 × 4 cm^2 cathode was applied and sintered. Due to the set-up for cell testing, the cells have an active electrode area of 16 cm^2. The set-up for cell testing, i.e. alumina housing, current collectors (Ni and Au foil), glass seals and Ni/YSZ and LSM based gas distributors, has been illustrated and described in detail elsewhere.[21,22]

Test procedure and operating conditions.— The cells were heated (1°C/min) to 1000°C for sealing and the NiO was subsequently reduced. The description of the cell test start-up sequence can be

*Electrochemical Society Active Member.
[z]E-mail: hauc@dtu.dk

found elsewhere.[21] After initial characterization consisting of polarization curves and electrochemical impedance spectroscopy (EIS) at a series of different gas compositions fed to the anode and cathode, respectively, at 750°C, 800°C and 850°C, the temperature was then fixed at 850 °C and the gas to the anode was changed to a $CH_4/H_2O/H_2$:30/60/10 gas mixture. For comparison with a previous study on similar cells, the total flow to the anode was set to 10 l/h (i.e. 3 l/h CH_4, 6 l/h H_2O and 1 l/h H_2 in the gas inlet tubing for the anode) for test at 1 A/cm^2 and for higher current densities the gas flows were scaled with the current density in order to keep the same fuel utilization i.e. a fuel utilization of 51%.[5] The addition of H_2S to the fuel inlet gas will affect the reformate gas equilibrium as reported by Rasmussen and Hagen and upon addition of 2 ppm H_2S the CH_4 conversion degree will be decreased and a fuel utilization of approximately 70% can be expected at the chosen test conditions.[23] OCV was checked before starting the test under current load. It was observed that complete internal reforming was obtained, since OCV values of ∼988–992 mV correspond to the reformed equilibrium gas mixture of $H_2/CO/H_2O/CO_2$:65.6/15.5/15.6/3.2 ($OCV_{theo.}$ = 994 mV for full reforming at 850 °C, without leaks) before and after the long-term tests under current load. At these test conditions the carbon activity was calculated to be 0.04. After reaching the desired current density the cells were left at for 55 to 70 hours at constant conditions to observe possible change in cell performance prior to H_2S exposure. The cell voltages changed less than 4 mV during this period of cell testing. Hereafter; 2 ppm H_2S (by dilution of a 200 ppm H_2S in H_2) was added for approximately 500 h. Sulfur addition was then stopped and the cells were left to recover at a constant current load. For the H_2S-free test the anode gas composition was set to H_2/H_2O:80/20, which corresponds to the same inlet oxygen potential (pO_2) as that obtained via complete reforming of a $CH_4/H_2O/H_2$:30/60/10 mixture. This gives the same "driving force" at the gas inlet; however the anode polarization losses are different in reformate gas, but this gives a similar starting point in terms of "driving force" while avoiding possible impurities from the methane gas feed.

Analysis of cell test data.— Figure 1 provides a schematic of the cell voltage curve over time for these tests and illustrates the data used for evaluating the cell voltage changes. The voltage change from *t*1 to *t*2 is denoted, $\Delta V_{init.}$, and typically *t2-t1* ∼ 10–30 h. The maximum cell voltage loss, ΔV_{max}, is between *t*1 and *t*3, cell voltage recovery, ΔV_{recov}, is between t_3 and t_4. The irreversible cell voltage drop, $\Delta V_{irrev.}$ is thus ΔV_{max}-ΔV_{recov} i.e. the ΔV_{irrev} is calculated as the cell voltage measured under current load immediately prior to H_2S exposure minus the cell voltage after recovery after H_2S addition has been stopped but still operated under constant current load. To calculate the long-term degradation rates during long-term testing, the voltage change over the last 200 h of H_2S poisoning was used.

Electrochemical impedance spectroscopy (EIS).— A Solartron 1255 frequency analyzer was used and impedance spectra (IS) were recorded from 96 kHz to 0.1 Hz with 12 points/decade. Analysis via distribution of relaxation times (DRT) at different test conditions (see Figure 1) was used to assist in the break-down of losses for the recorded IS. For quantitative analysis of the IS complex-non-linear-least-squares (CNLS) method was used to fit an equivalent circuit model to the data. For a quantitative break-down of losses via IS the equivalent circuit model depicted in Figure 1 was applied. This equivalent circuit is based on the work reported by Barfod et al.[24] and Kromp et al.,[25] in which the electrochemical impedance response from the Ni/YSZ and LSM/YSZ electrodes have been approximated by two RQ-elements (Voigt-elements) each. The higher frequency impedance arc $(RQ)_{high}$ at ∼20–40 kHz has contributions from both electrodes and has previously been ascribed to the coupled charge transfer and ionic transport through the ionic conducting matrix in the electrodes which can also be described in more detail via transmission line models for the impedance response.[26–30] Characteristic frequencies for the individual contributions to the IS can be found in the frequency decades sketched in Figure 1, with the summit frequency for $(RQ)_{Ni\text{-}TPB}$ being slightly lower (∼ 3 kHz) during testing under current load than at OCV. The software ZView 3.2[31] was used to CNLS fit a model to the experimental IS and in-house developed software RAVDAV[32] was used for DRT analysis of the IS.

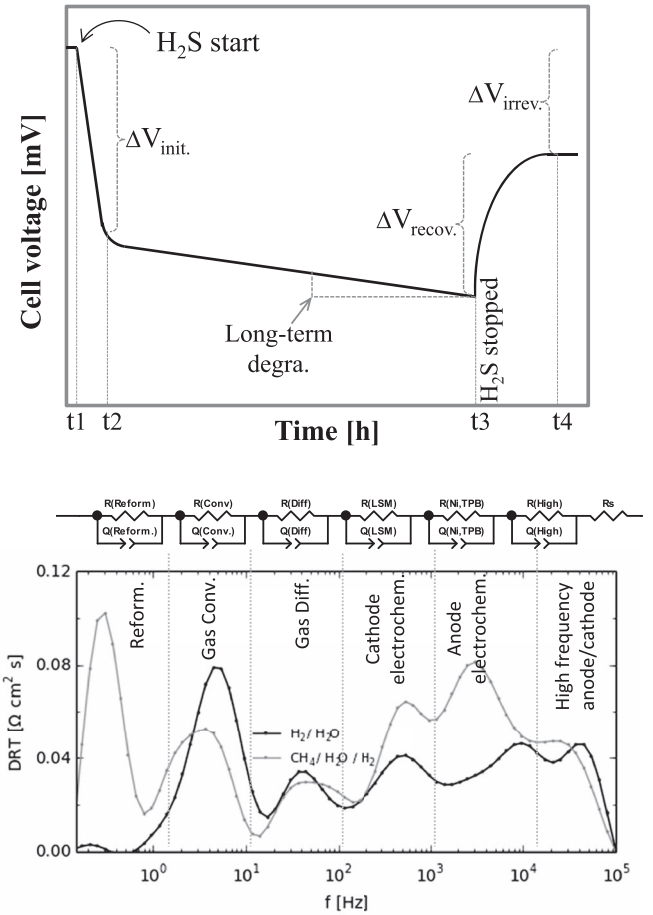

Figure 1. Schematic of a cell voltage curve during galvanostatic fuel cell testing and H_2S poisoning (top) and of applied equivalent circuit for the Ni/YSZ-YSZ-LSM/YSZ cells together with a distribution of relaxation times plot (DRT,)[26] of IS applying H_2/H_2O or $CH_4/H_2O/H_2$ at OCV and 850°C illustrating characteristic frequencies ranges for different processes (bottom).

SEM imaging and image analysis.— Pieces of a cross section length of ∼ 1 cm of the tested cells were prepared for SEM investigations by vacuum embedding in epoxy (EpoFix from Struers) followed by grinding and polishing. A Zeiss Supra 35 FE-SEM (Field Emission Gun Scanning Electron Microscope) was used for imaging. SEM images obtained at 10 kV using the secondary electron detector and low-voltage SEM images were obtained at 0.9 kV using the in-lens detector. Low-voltage in-lens SEM imaging allows percolating and non-percolating Ni to be distinguished in the Ni/YSZ cermet microstructure, as described by Thydén et al.[33]

Image analysis by line-intercept-method[18] allowed the determination of the area fraction of percolating Ni and pores, using the in-house developed Matlab based software, ManSeg. For each sample, 15 recorded images at a magnification of 4 kX were used for the analyzes of percolating Ni and porosity; corresponding to analyzes of an anode/electrolyte interface of more than 1500 μm for each cell.

Results and Discussion

Cell voltage curves as a function of time – degradation overview for sulfur tests.— Table I lists test acronyms, cell and test specifications, along with a summary of the test results in form of cell voltage changes

Table I. Overview of cell and test specifications and voltage changes. Description of the different voltage changes is sketched in Figure 1. η is the cell overpotential at start of H_2S exposure. *YSZ-Hi-Spr* had a sprayed electrolyte and active anode while the rest of the cells have tape cast electrolyte and active anodes. "Low overpotential" tests are given in italic.

Test acronym	Cell specifications	i (A/cm^2)	η (mV)	$\Delta V_{init.}$ (mV)	ΔV_{max} (mV)	Long-term degr. (mV/kh)	Long-term degr. (mΩcm^2/kh)	$\Delta V_{recov.}$ (mV)	$\Delta V_{irrev.}$ (mV)
YSZ-Hi-Spr[1]	YSZ-based cell	1	320	100	216	225	225	105	111
ScYSZ-Low[1]	*Sc-Y co-doped ZrO_2*	*1*	*237*	*61*	*85*	*0*	*0*	*75*	*10*
YSZ-Low	*YSZ-based cell*	*1*	*209*	*93*	*109*	*10*	*10*	*102*	*7*
YSZ-Hi	YSZ-based cell	1.38	291	121	208	180	131	130	78
YSZ-no-S	YSZ-based cell, LSC/CGO cathode and CGO barrier layer	1.88	360	-	-	15	8	-	-

[1]Test reported by Hagen et al.[5] in which the tests where denoted "Ni,YSZ,LSM" and "Ni,ScYSZ,LSM", respectively.

and long-term degradation rates. The cell with the sprayed electrolyte and sprayed active anode produced in our lab will typically have a slightly more porous anode compared to the cells with tape cast anodes which have porosities of ∼ 14% in the active anode in the reduced state.[18]

Figure 2 shows the corresponding cell voltage curves as a function of time for the four H_2S poisoning tests and the H_2S free test. *YSZ-Hi-Spr* and *ScYSZ-Low* were previously reported by Hagen et al.,[5] and are included here for comparison. In the article by Hagen et al. these tests were denoted "Ni,YSZ,LSM" and "Ni,ScYSZ,LSM", respectively. The sulfur tests can be divided into two groups regarding long-term degradation behavior during H_2S exposure: Group I- tests with marginal long-term degradation (*ScYSZ-Low* and *YSZ-Low*); and group II- tests with significant, more or less linear, long-term degradation (∼ 131–276 mΩcm^2/kh, for *YSZ-Hi-Spr* and *YSZ-Hi*). This general trend regarding long-term degradation behavior can be related to one parameter, the cell overpotential (η) or perhaps more specifically the anode overpotential, which is low for group I and high for group II; while the cell compositions (YSZ vs. ScYSZ), microstructure i.e. anode porosity or specific current density obviously are less important parameters, when it comes to the long-term degradation behavior upon H_2S exposure. Parameters such as anode microstructures and current density can therefore be considered *indirect* parameters when it comes to initiating the irreversible long-term degradation upon H_2S exposure as the eventually dictate the anode overpotential. As reported previously, a tape cast Ni/ScYSZ based cell showed similar high degradation rates for the long-term degradation as the Sc-free *YSZ-Hi-Spr* and *YSZ-Hi* (in this work) upon H_2S poisoning tested under similar conditions at high overpotential.[11]

The irreversible cell voltage loss after stopping the H_2S poisoning and recovery (still under current load) is only ∼ 7–10 mV for group I tests, while the high overpotential sulfur tests, i.e. group II tests, have irreversible cell voltage losses that are ∼10 times larger (see Table I).

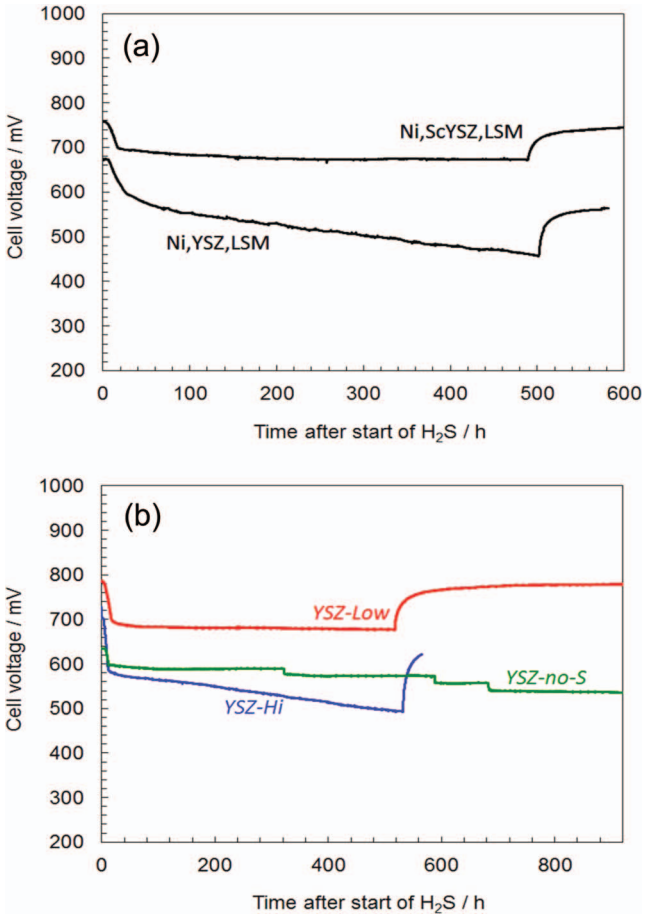

Figure 2. Cell voltage curves as a function of time at 850°C, $CH_4/H_2O/H_2$:30/60/10 for *YSZ-Hi-Spr* denoted Ni,YSZ,LSM and *ScYSZ-Low* denoted Ni,ScYSZ,LSM (top, reprint from).[5] Cell voltage curves as a function of time for *YSZ-Low* (red), *YSZ-Hi* (blue) and *YSZ-no-S* (green) (bottom). For *YSZ-no-S* (green) the anode inlet gas composition was H_2/H_2O = 0.8/0.2. Overview of cell and test specifications is given in Table I.

Cell voltage as a function of time – sulfur free test.— Figure 2 also includes the cell voltage curve for the high overpotential test with no H_2S added i.e. the *YSZ-no-S* test. The cell used for the *YSZ-no-S* has anode half-cell identical to the cells used for the *YSZ-high* and *YSZ-low* tests. To reach a similar high overpotential in the H_2S free test, the current density was increased to 1.88 A/cm^2 for *YSZ-no-S* (t = 0 h in Figure 2). Due to H_2 flow limitations of the used test rig the current density could not be increased further while keeping the gas mixtures and fuel utilization equivalent to previous tests. The cell overpotential for *YSZ-no-S* was therefore increased further by decreasing the temperature by 30°C and subsequently three times by 10°C. The H_2S-free test, *YSZ-no-S*, had a degradation rate of only 15 mV/kh (8 mΩcm^2/kh) for the last 200 h of testing, while the equivalent cell of test *YSZ-Hi* degraded 180 mV/kh (131 mΩcm^2/kh) during the last 200 h of H_2S poisoning. This strongly indicates that the observed irreversible degradation for the high overpotential tests *YSZ-Hi-Spr* and *YSZ-Hi* and for the *ScYSZ-Hi* reported previously[11] must be closely related to the presence of H_2S, even at such relatively low concentrations of 2 ppm. The significantly lower long-term degradation rate for the *YSZ-no-S* compared to *YSZ-Hi* could simply be an effect of changing to H_2/H_2O fuel instead of $CH_4/H_2O/H_2$ fuel, as used for the *YSZ-Hi* and thereby not solely related to the absence of H_2S. However, this is not likely when considering the long-term degradation results for non-H_2S tests at high current and high overpotential at

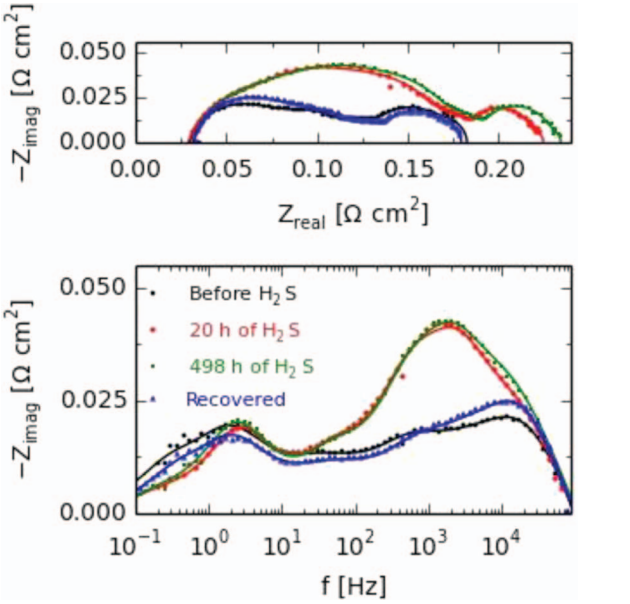

Figure 3. IS recorded for *YSZ-Low*. Lines represent results of the CNLS fitting using the equivalent circuit model in Figure 1. Results from the CNLS fitting are given in Table II. Test conditions were: 1.00 A/cm^2, 850°C, inlet anode gas composition $CH_4/H_2O/H_2$:30/60/10 and air to the cathode.

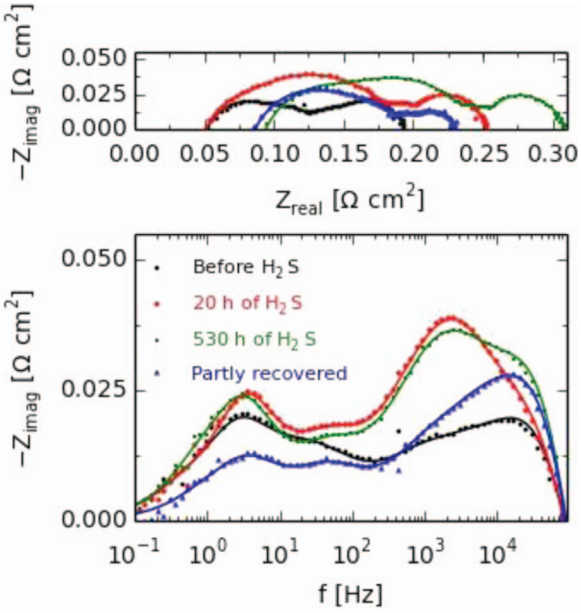

Figure 4. IS recorded for *YSZ-Hi*. Lines represent results of the CNLS fitting using the equivalent circuit model in Figure 1. Results from the CNLS fitting are given in Table III. Test conditions were: 1.38 A/cm^2, 850°C, inlet anode gas composition $CH_4/H_2O/H_2$:30/60/10 and air to the cathode.

850°C reported previously by Hagen et al.[13] In this work Hagen and co-workers reported degradation rates in the order of 10–20 mV/kh (∼10 mΩcm^2) for long-term H_2S-free tests operated at 850°C also applying methane containing fuels (internal reforming conditions) for 1500 h at high current densities giving rise to cell overpotentials of ∼300–400 mV. To summarize, the long-term degradation rate for the high overpotential test *YSZ-no-S* (anode half cell identical to the cells used for the *YSZ-Hi* and *YSZ-Low* tests, but anode gas compositions) and for the previously reported high overpotential sulfur-free test reported by Hagen et al. (internal methane reforming gas conditions) are similar and both in the range of 10–20 mV/kh, while the long-term degradation rate for *YSZ-Hi* is significantly different as it is a factor of ∼ten times larger.

The subsequent analyzes of the process specific impedance contributions and postmortem SEM analyzes were divided into three: 1) Low cell overpotential H_2S cell test, 2) high cell overpotential H_2S cell test, and 3) high cell overpotential H_2S-free cell test.

Low overpotential H_2S test – EIS.— Figure 3 shows the IS recorded at *t1*, *t2*, *t3* and *t4* for the low overpotential test *YSZ-Low* where a current density of 1 A/cm^2 was applied. Table II gives an overview of the resistances determined by CNLS fitting of the equivalent circuit model depicted in Figure 1 to the measured impedance data. Only negligible variation of the ohmic resistance was observed during the entire test. Upon start of H_2S addition the impedance response in the frequency range 1–3 kHz increases significantly corresponding to an increase in the resistance associated with the charge transfer reaction at the TPB in the anode, $R_{Ni\text{-}TPB}$, denoted "Anode electrochem" in Figure 1. $R_{Ni\text{-}TPB}$ increases by a factor of 8 within ∼ 24 h of H_2S exposure. However, during the subsequent 480 h of testing with an exposure of 2 ppm H_2S to the anode, $R_{Ni\text{-}TPB}$ remains constant. When H_2S addition was stopped and the cell was left to recover (still under current load) $R_{Ni\text{-}TPB}$ decreased almost to the pre-H_2S exposure value. Furthermore, a small increase in the impedance at high frequency (20–40 kHz) is observed over these 500 h of H_2S poisoning, corresponding to an increase in R_{high}.

In the work by Hagen et al.[5] it was discussed whether the increased long-term stability for *ScYSZ-Low* compared to *YSZ-Hi-Spr* upon H_2S-poisoning could be an effect of the scandia-doping, which will lead to increasing ionic conductivity compared to the YSZ-based cells and changes in the wettability and bonding of Ni on the ceramic backbone.[34,35] The results in this work are remarkable as the Ni/YSZ-based (i.e. Sc-free) cell used for *YSZ-Low*, seems equally long-term stable during H_2S poisoning when compared to the Ni/ScYSZ-based cell in the *ScYSZ-Low* test when the two cells are tested at similar low overpotential.

High overpotential H_2S test – EIS.— Figure 4 shows the IS recorded at *t1*, *t2*, *t3* and *t4* for the high overpotential test *YSZ-Hi* i.e. a cell similar to the one used in *YSZ-Low* test but now applying a current density of 1.38 A/cm^2. Table III gives an overview of the resistances obtained from CNLS fitting the IS in Figure 4 based on CNLS fit to the experimental data applying the equivalent circuit model depicted in Figure 1. From the results in Table III it can be seen that the high overpotential test, *YSZ-Hi*, basically exhibits the same trend regarding $R_{Ni\text{-}TPB}$, as observed for the low overpotential test, *YSZ-Low*. The striking difference between this high overpotential test (*YSZ-Hi*) and the previous low overpotential test (*YSZ-Low*) is that the ohmic

Table II. Results from CNLS fitting of IS shown in Figure 3 for *YSZ-Low* i.e. low overpotential test H_2S-test. The equivalent circuit model applied for fitting is sketched in Figure 1. Estimated uncertainty for calculated resistances is ∼4 mΩcm^2.

Time	R_s (mΩcm^2)	R_{high} (mΩcm^2)	$R_{Ni\text{-}TPB}$ (mΩcm^2)	$R_{LSM,low}$ (mΩcm^2)	R_{Diff} (mΩcm^2)	$R_{Conv.}$ (mΩcm^2)	$R_{Reform.}$ (mΩcm^2)
Before H_2S (*t1*)	23	55	6	28	22	34	15
Inflect. point (*t2*)	23	50	48	44	19	34	6
498 h H_2S (*t3*)	26	62	45	40	18	37	6
Recovery (*t4*)	27	58	12	19	22	28	13

Table III. Results from CNLS fitting of IS shown in Figure 4 for *YSZ-High* i.e. high overpotential H_2S-test. The equivalent circuit model applied for fitting is sketched in Figure 1. Estimated uncertainty for calculated resistances is ∼4 mΩcm².

Time	R_s (mΩcm²)	R_{high} (mΩcm²)	$R_{Ni\text{-}TPB}$ (mΩcm²)	$R_{LSM,low}$ (mΩcm²)	R_{Diff} (mΩcm²)	$R_{Conv.}$ (mΩcm²)	$R_{Reform.}$ (mΩcm²)
Before H_2S (*t1*)	39	59	11	18	29	33	6
Inflect. point (*t2*)	35	59	58	28	24	42	7
530 h H_2S (*t3*)	70	83	56	27	20	39	12
Recovery (*t4*)	60	90	17	18	18	20	*

*Noise in the IS at frequencies below 1 Hz. Therefore no break-down of losses and CNLS fit for impedance data below 1 Hz.

resistance (R_s) and the high frequency contribution to the polarization resistance (R_{high}) increase over the entire sulfur poisoning test period for *YSZ-Hi* and did not recover after stopping the H_2S addition i.e. *YSZ-Hi* experiences an irreversible loss of performance.

Analyzes of the four IS recorded for *YSZ-Hi-Spr* at *t1*, *t2*, *t3* and *t4* (IS shown by Hagen et al.)[5] show the same trends as the results given in Table III for *YSZ-High* (Table II in).[11] That is; R_s and R_{High} increase (irreversibly) during the long-term H_2S exposure.

Using the results from CNLS fitting of IS (Table II and Table III) one can estimate the anode overpotentials (see Supplementary Material) during testing with H_2S-exposure. At the inflection point (*t2*) the anode overpotential can be estimated to be ∼ 132 mV for *YSZ-Low* which does not initiate significant long-term irreversible degradation; whereas the anode overpotential at *t2* for *YSZ-Hi* can be estimated to be ∼ 221 mV which evidently entail significant long-term irreversible degradation.

Comparison of *YSZ-Low* and *YSZ-Hi* illustrates that by "pushing" the otherwise high performing and sulfur tolerant tape cast laminated Ni/YSZ anode half-cell (*YSZ-Low*) to a higher overpotential, and especially higher anode overpotential (*YSZ-Hi*), the cell can be forced to a largely irreversible "degradation-regime", where an almost linear degradation of the cell takes place upon addition of only 2 ppm H_2S in the fuel gas ($CH_4/H_2O/H_2$:30/60/10) at 850°C. Cells with Ni/Sc(Y)SZ anodes have been reported to be more sulfur tolerant than Ni/YSZ anodes.[5,7] However, *ScYSZ-Hi* reported in our previous work[11] shows that Ni/ScYSZ-based cells can likewise be "pushed" into a long-term degradation regime at similar conditions (gas and temperature) through increased cell overpotential. Consequently, the long-term irreversible degradation for the sprayed Ni/YSZ-based cell, *YSZ-Hi-Spr*, originally reported by Hagen et al.[5] compared to the more stable tape cast laminated and Sc-doped cell (*ScYSZ-Low*) was not merely a question of ScYSZ versus YSZ, although this difference in composition, together with microstructural differences, can play a role in the initial cell performance loss and the cell overpotential "threshold" at which the irreversible long-term degradation is initiated. The results reported here point toward that the observed long-term and irreversible degradation during these long-term poisoning tests at 850°C and internal reforming gas mixture to the anode is triggered by, and closely related to, the overpotential upon start of the H_2S poisoning. The IS analyzes for the high overpotential tests (*YSZ-Hi-Spr*, *YSZ-Hi* and *ScYSZ-Hi*)[11] reveals that the long-term degradation (from *t2* to *t3*) also constitutes the irreversible part of the lost performance.

High overpotential H_2S-free test –EIS.— Due to the nature of the test sequence for the *YSZ-no-S* test it is not possible to show IS at times corresponding to *t1*, *t2*, *t3* and *t4* as given in Figure 3 and Figure 4 for *YSZ-low* and *YSZ-Hi*, respectively. Figure 5 shows the first and the last IS recorded for this last part of the *YSZ-no-S* test i.e. at t = 675 h and t = 900 h in Figure 2. This verifies that the stable cell voltage over the last approximately 225 h at constant test conditions for the *YSZ-no-S* is due to cell stability and not due to counteracting resistance changes within the cell. The LSC/CGO cathode will give rise to an impedance response with a summit frequency ∼ 100 Hz.[20] The IS in Figure 5 shows the stability of R_s and the high frequency part of R_p (R_{high}), in contrast to the development of the impedance observed from *t2* to *t3* for the *YSZ-Hi* test (Figure 4).

Post-mortem analysis of the anode layers.— Figure 6 shows representative low voltage in-lens SEM images of the anode/electrolyte interface for cells from the *YSZ-Low, YSZ-Hi, and YSZ-no-S* tests, where percolating Ni particles appear bright.[33] From the images in Figure 6 it is evident that the percolating Ni network for the *YSZ-Low* and *YSZ-no-S* looks similar, and with an acceptable fraction of percolating Ni in both the cermet anodes and support layers, when compared to non-tested reference cells.[18,36] In contrast, for the anode from the *YSZ-Hi* test there is a significant lack of percolating Ni in the 2–4 microns closest to the electrolyte, whereas the percolating Ni network in the region further away from the anode/electrolyte interface seems unaltered when compared to the anodes from the *YSZ-low* and *YSZ-no-S*. These observations are in accordance with the observations made by Hagen et al. for cell from the *YSZ-Hi-Spr* test.[5]

Quantification of the percolating Ni network, i.e. area fraction and number of percolating Ni particles/100 μm grid line, was obtained from the in-lens low voltage SEM images. When obtaining quantitative data for the *area fraction* of percolating Ni from the low voltage in-lens SEM images such as those given in Figure 6, attention should be paid to two issues associated with this type of measurement; 1) the percolation images do not take into account percolation through pathways in the part of the sample that has been polished away and 2) it has been reported that a slight over-estimate of the Ni fraction will occur due to charging effects as described and quantified elsewhere.[37] This means that the *accuracy* of the measurements is likely to be influenced by a small systematic (overestimation) error, but precision of the measurement is high due to the same reproducible methodology being applied to all samples. The measured fraction of percolating

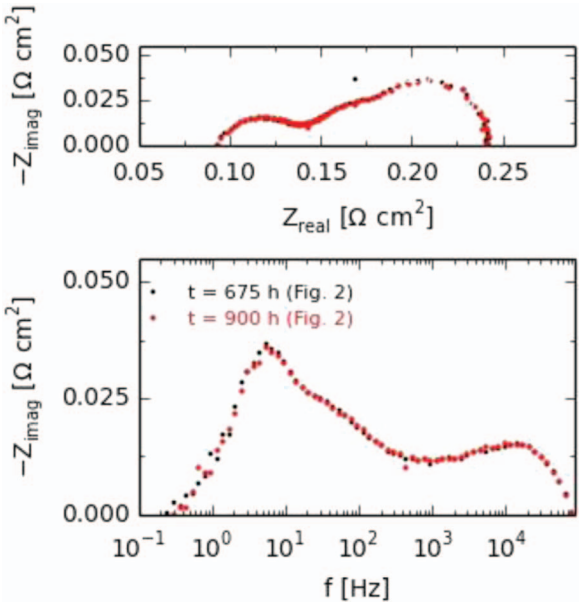

Figure 5. IS recorded for the *YSZ-no-S* test in the last test period i.e. corresponding to t = 675 h and t = 900 h in Figure 2 at constant test conditions i.e. 1.88 A/cm², 790°C, inlet anode gas composition $p(H_2)/p(H_2O)$ = 0.8/0.2, air to the cathode.

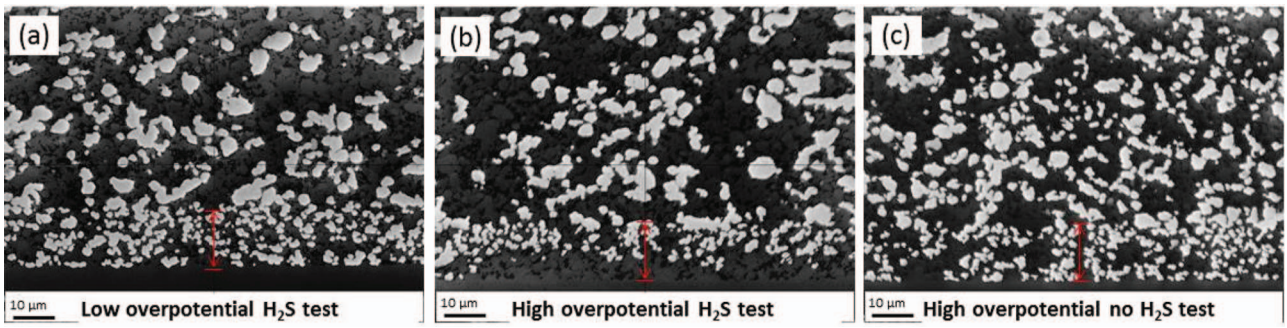

Figure 6. Low voltage in-lens SEM images of the anode/electrolyte interface for the cells from the *YSZ-low* (low overpotential H_2S test), *YSZ-Hi* (high overpotential H_2S test) and *YSZ-no-S* (high overpotential no H_2S test). The red bar indicates the thickness of the active anode i.e. the lower end of the bar marks the anode/electrolyte interface.

Table IV. Quantification of percolating Ni particles for long-term tested cells. *"Anode(electrolyte)"* refers to the anodes characterized with the intercept line approximately 0.5–1 µm from the electrolyte interface and *"Anode(anode sup.)"* refers to the anodes characterized with the intercept line approximately 0.5–1 µm from the anode support interface.

	Fraction of Percolating Ni		No. of Ni part./100 µm	
Test	Anode (electrolyte)	Anode (anode sup.)	Anode (electrolyte)	Anode (anode sup.)
YSZ-Low	0.27± 0.07	0.24± 0.03	15.7 ± 4.2	23.0 ± 2.7
YSZ-Hi	0.04 ± 0.02	0.34 ± 0.02	2.4 ± 1.2	26.2 ± 2.2
YSZ-no-S	0.33 ± 0.05	0.27 ± 0.04	22.9 ± 4.4	21.7 ± 3.1

Ni given in Table IV should thus be valid for a comparative study between the different tests in this work since the unknown accuracy error is expected to be the same for all samples. However the measured fraction of percolating Ni given in Table IV is not necessarily directly comparable with similar numbers for the fraction of percolating Ni given in literature. In this perspective the *number* of percolating Ni particles (or Ni agglomerate) per 100 µm grid line – instead of the *area fraction* - is a valuable and simple parameter for comparison with other studies.

Table IV gives a summary of the quantitative analysis of the area fraction of percolating Ni and the number of percolating Ni particles/100 µm grid line for anodes from the three tests, *YSZ-low*, *YSZ-Hi* and *YSZ-no-S* near the anode/electrolyte interface and near the anode/anode support interface. Clearly, the *YSZ-Hi* cell has much lower number of percolating Ni particles in the inner most 2–4 µm of the anode.

When viewing the low voltage in-lens SEM images of the cell from the *YSZ-Hi* test, the changes in the microstructure correspond to "extending" the dense YSZ electrolyte by 2–4 µm with an extra porous YSZ layer. These observations fit well with the irreversible R_s increase observed in the IS in Table IV for *YSZ-Hi* during the long-term degradation. Furthermore, it is hypothesized that the thickness of this percolating Ni depleted anode layer will increase with increasing test time, at conditions where irreversible long-term degradation dominates (*t2* to *t3* Figure 1 and Figure 2). This in turn implies 1) that for two identical microstructures the long-term degradation rate for cells with a better ion-conductor such as ScYSZ[38] as anode skeleton can be expected to be lower, when compared to a YSZ-based cell and 2) for electrolyte supported cells a "sudden death" of the anode, e.g. as observed by Sasaki and co-workers,[7] can be expected when the depleted layer thickness equals the total thickness of the anode. The long-term degradation behavior can, from this perspective, be expected to be different for anode supported.

The loss of percolating Ni network, both in terms of area fraction and number of percolating Ni particles, in the innermost few microns of the anode for the *YSZ-Hi* cell (Figure 6b), can be caused by several different phenomena: 1) buildup of impurities in between Ni particles),[39,40] 2) nano-scale Ni morphology changes 3) evaporation as Ni-hydroxide species[41] and 4) diffusion of Ni).[41,42] In case 1 and 2 the Ni will still be present more or less in its original position in the anode structure however it will not be electrochemically active. In case 3 and 4 there will be a decrease in the total Ni area fraction and this must be accompanied by an increase in the pore phase fraction. Therefore, investigation of the pore phase in the innermost part of the anode layers can provide an indirect measure of decreased Ni fraction and avoids the challenges and uncertainties related to automated segmentation and quantification of the Ni and YSZ phases from higher voltage SEM images.[43,44]

Figure 7 shows representative SEM images of the anode/electrolyte interface for the cells used in *YSZ-Low*, *YSZ-Hi* and *YSZ-no-S* tests. It

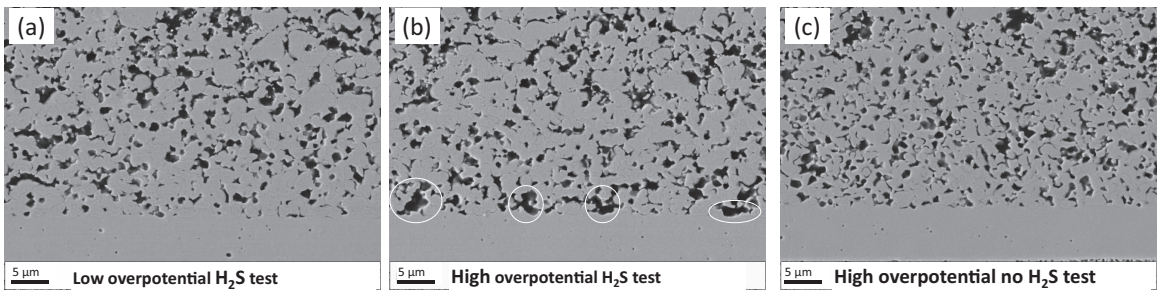

Figure 7. Representative SEM images at an acceleration voltage of 10 kV for polished cross-sections of anode/electrolyte interfaces for the tested cells from (a) *YSZ-Low* test, *(b) YSZ-Hi* test and (c) *YSZ-no-S* test. Circles indicate large porosities in the innermost few microns of the cell from the *YSZ-Hi* test.

Table V. Quantification of porosities in the anodes for long-term tested cells. "Anode(electrolyte)" refers to the anodes approximately 0.5–1 μm from the electrolyte interface. Reference cell refers to a reduced, but not long-term tested cell previously reported.[18]

Test	Pore fraction Anode(electrolyte)	No of pores/100 μm Anode(electrolyte)
Reference cell*	0.14	30.6
YSZ-Low	0.15 ± 0.03	27.1 ± 3.1
YSZ-High	0.29 ± 0.04	30.6 ± 3.5
YSZ-no-S	0.18 ± 0.02	31.7 ± 3.8

*Data from Hauch et al.[18]

can be observed that the anode from the *YSZ-Hi* test has a significant number of larger pores close to the anode/electrolyte interface, if compared to the anodes from *YSZ-low* and *YSZ-no-S* test. These are indicated by the circles in Figure 7b. The porosity change is mainly caused by some larger pores within the 2–4 μm of the anode layer closest to the electrolyte.

Table V gives a summary of the quantification of pore area fraction and number of pores on a grid line 0.5–1 μm from the anode/electrolyte interface. From Table V it is evident that the *number* of pores is similar for the investigated anodes, but the pore area *fraction* is significantly increased for the anode from the *YSZ-Hi* test. There is striking correlation between the low number of percolating Ni particles (Table IV) and the increased pore fraction (Table V) for the anode from the *YSZ-Hi* test compared to the anode from the *YSZ-low* test. Based on the numbers in Table IV a 100 μm anode/electrolyte interface of the cell from the *YSZ-Hi* test will typically have ∼13 percolating Ni particles less than the anode from the *YSZ-Low* test. The mean-intercept-length for Ni particles in long-term tested SOFC produced in our lab is ∼1.1–1.2 μm,[14,24] which fits well with the observed increase in porosity (∼ 14 μm/100 μm intercept length) for the cell from the *YSZ-Hi* test when compared with cell from the *YSZ-Low* test.

Even though it is clear from these SEM images and image analyzes that the innermost few microns of the anode from the *YSZ-Hi* test has a decreased Ni content, it has not been possible to locate and quantify this Ni elsewhere in cell; however it could be present in the 300 μm thick anode support layer and if well distributed it will be hard to quantify this additional Ni content in the 300 μm thick anode support layer.

To summarize, the SEM results show that the irreversible long-term degradation has led to significant structural changes even on the micrometer scale. The migration of Ni from the anode/electrolyte interface excludes the possibility of "re-activation" of the Ni catalyst as it is no longer present in the required positions in the anode. Furthermore, the corresponding increase in the fraction of porosity in the anode/electrolyte interface will inevitably change the mechanical properties of this interface.

Figure 8 shows higher magnification SEM images of the part of the anode closest to the electrolyte for the *YSZ-Hi* test. The features observed in Figure 8 can be found in numerous places in the anode-electrolyte interface region of the cell from the *YSZ-Hi* test. The curvature and size of the right side of the pore seems to indicate an empty space left over by a now missing Ni particle as the "rounded" shape of the pore is different from the more "fractured" pores formed by the YSZ grains. The higher magnification SEM image (Figure 8b) of this pore also reveals the presence of nano-sized particles along this round-shaped part of the pore. Energy dispersive spectroscopy (EDS) has been obtained in the region where these nano-particles are present and in regions of pores/YSZ interfaces where no nano-particles could be observed in the SEM images. These EDS measurements reveal that the observed nano-particles contain Ni and traces of sulfur either in, on or in the vicinity of these nano-particles.

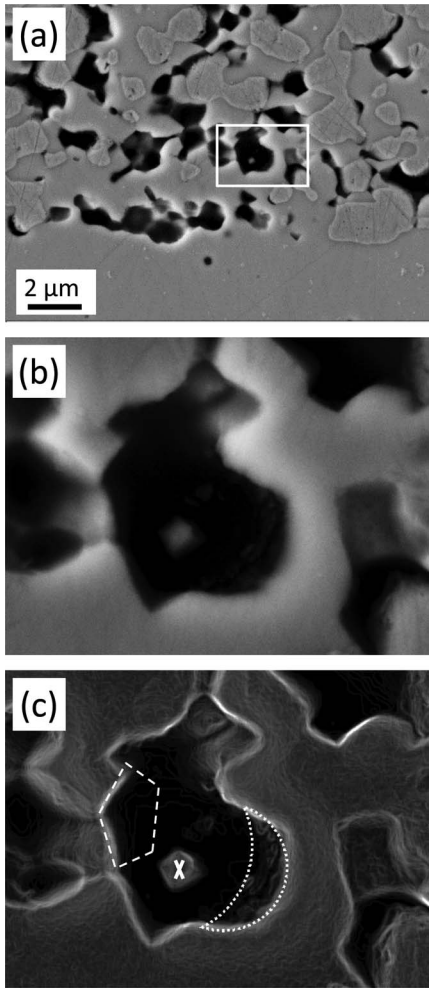

Figure 8. a) Secondary electron SEM images of nano-particles in pore of the *YSZ-Hi* (high overpotential test with H_2S addition); b) higher magnification images of the region marked by the square in a) and c) highlighting nano-particles in the pore. Dotted line ("moon-shaped") marks a region in the pore where nano-particles are observed and analyzed by point EDS and dashed line ("pentagon") marks a region of the pore analyzed by point EDS but where no nano-particles could be observed. The particle marked by "X" is an YSZ particle.

Sulfur initiated long-term degradation at high cell overpotential.— Yoshizumi and co-workers suggested that it is the increased current density (increased oxygen ion flux) that promotes Ni surface oxidation and used this as argument for what "triggers" the observed irreversible long-term degradation that they reported.[10] The fact that we do not observe irreversible performance loss in the YSZ-no-S test, but we do observe this in the YSZ-Hi test, points to that this is not the controlling mechanism causing irreversible loss. Based on the results reported here we propose that it is the *combination of the continued feed of H_2S and the high overpotential* (i.e. high oxygen potential) that is initiating the observed irreversible long-term degradation.

To estimate an average oxygen potential (pO_2) in the anode compartment of the cells at a given time during test we use the results from the break-down of losses obtained from analyzes of IS.[45] At *t2*, where the initial fast, but mainly reversible, passivation of the cell is completed and the long-term irreversible degradation becomes dominating for the *YSZ-Hi* test, the $pO_{2\text{-anode-compartment}}$ is calculated to be $\sim 4 \times 10^{-17}$ atm and only $\sim 6 \times 10^{-18}$ atm for *YSZ-Low* (Table II and Table III). The calculation of the $pO_{2\text{-anode-compartment}}$ is based on the overpotential on the anode side of the cell calculated from the resistance contributions attributed to the anode half-cell i.e. the total resistance minus the ohmic resistance (R_s), the cathode resistance

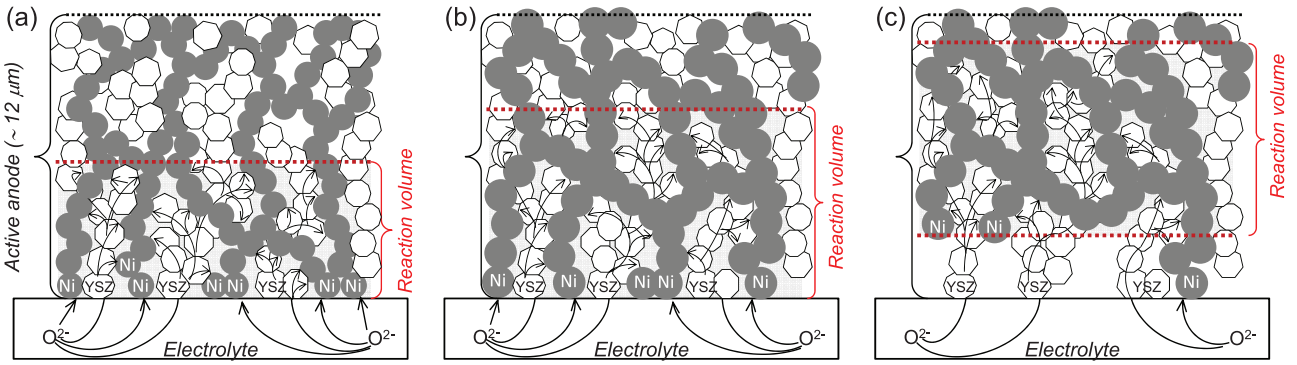

Figure 9. a) Sketch of the Ni/YSZ anode microstructure at start of test; b) after long-term test either with sulfur exposure at low overpotential i.e. *YSZ-Low* or at high overpotential without H_2S exposure i.e. *YSZ-no-S*; and c) after high overpotential test with H_2S exposure and irreversible loss in performance observed i.e. *YSZ-Hi*.

(R_{LSM}) and half of the R_{high}; all determined from the analysis of IS. A pO_2 of 4×10^{-17} atm in the anode compartment locally is not sufficiently high for Ni oxidation to occur at 850°C which can be expected at a pO_2 around 10^{-13} atm.[45] Based on thermodynamic calculations and the overall cell test conditions (i.e. externally controlled conditions such as set temperature and fuel composition) one should not expect formation of nickel sulfide (Ni_3S_2) either.[3,7,46,47] However, the given test conditions and values for $pO_{2\text{-anode-compartment}}$ are "overall" numbers for the entire anode utilization volume and do not provide information on exact conditions on the nanometer scale of the anode at – or in the nano-scale vicinity of - the TPB at which the pO_2, gas composition and temperature can be significantly different. Kishimoto and co-workers reported that the Ni-S system is complex and includes Ni-S eutectics between Ni and Ni_3S_2 and showed thermodynamic data for the significant increase (~ doubling) of the solubility of oxygen and sulfur in Ni when increasing the oxygen potential, pO_2, by one order of magnitude.[3] Furthermore, work by Lohsoontorn et al.[48] indicates that the presence of sulfur will give rise to increased Ni diffusion and sintering. These reported data render it probable that O and S solubility, Ni sintering and Ni diffusion will be affected by high oxygen potential and sulfur exposure. This will inevitably lead to enhanced mobility of Ni in the active anode thus potentially enhanced close to the anode-electrolyte interface where the highest oxygen potential is present. Finally it should be noted that a high pO_2 locally in the vicinity of the TPB can lead to significant quantities of Ni^{2+} to be present in YSZ,[49] which will affect the ionic conductivity of the YSZ skeleton[50,51] and in turn can be expected to lead to an increase in the impedance at high frequencies (above ~ 15 kHz,).[26,27]

To summarize our findings and combine the impedance analyzes results with the post-mortem SEM results Figure 9 shows a sketch of the initial state of the Ni/YSZ anode microstructure (Figure 9a), and after long-term test with no irreversible degradation i.e. test *YSZ-Low* and *YSZ-no-S* (Figure 9b) and after long-term test with sulfur exposure at high overpotential with irreversible degradation i.e. *YSZ-Hi* test (Figure 9c). In the initial state (Figure 9a), the Ni particles are well distributed and a well percolating network exists. This means a high TPB density in the few microns of the anode closest to the electrolyte and O^{2-} ions will find a TPB at the anode/electrolyte interface or only need to be conducted few microns in the YSZ skeleton of the anode. In other words; the utilization volume is expected to be contained within the innermost 5–10 μm of the anode.[52,53] Figure 9b illustrates the anode microstructure after test *YSZ-Low* and *YSZ-no-S*. In both cases Ni coarsening has occurred, but there is still a well percolating Ni network present in the entire anode. The coarsening of the Ni particles means a slightly lower TPB density per given nominal electrode volume which in turn corresponds to a slightly expanded reaction volume, and we can expect the electrode area corrected $R_{Ni,TPB}$ to have increased slightly which was also observed from the analyzes of IS. However in the anode structure of Figure 9b the YSZ skeleton and the percolating Ni network in the innermost part of the anode is still intact which in turn means that the O^{2-} ions still have a short path to be conducted to find an active TPB, and the high frequency part of the impedance response (R_s and R_{high}) should therefore not have changed significantly for the structure in Figure 9b. This was also observed from the IS from the *YSZ-Low* and *YSZ-no-S* test. The observed slight increase in $R_{Ni\text{-}TPB}$ for *YSZ-Low,* even after long recovery time, can also be partly due to traces of Ni-S species still being present in the anode structure but not detectable via SEM/EDS. Such traces of sulfur need to be investigated by e.g. TEM/EDS and/or ToF-SIMS as illustrated by Schubert and co-workers.[54] Figure 9c illustrates the Ni/YSZ anode after long-term H_2S exposure at high overpotential. In this degraded anode, a percolating Ni network is lacking in the 2–4 μm of the anode layer closest to the electrolyte. This irreversible change means that the O^{2-} ions now have a longer path to reach an active TPB in the anode, which in terms of expected impedance response fits well with the observed irreversible increase in R_s for *YSZ-Hi.* The electrochemical reactions will now take place significantly further away from the electrolyte. Furthermore, in this outer layer of the anode, the Ni particles have coarsened as well, leading again to an increased reaction volume compared to that of the initial anode. In terms of impedance response these should lead to a slight irreversible increase in $R_{Ni\text{-}TPB}$ even in the case where all surface adsorbed sulfur species desorb from the Ni particles. For an anode supported cell the reaction utilization volume can in principle extend into the anode support layer either if the long-term test period is prolonged or in case thinner active anodes are applied and will become limited by the ionic conduction in the porous YSZ network especially if the reaction utilization volume is to be extended to the anode support layer in which 3YSZ is used. To investigate these effects further cell tests with anode thickness variations in line with those reported by Park and co-workers could provide valuable information regarding the long-term irreversible degradation.[55]

From the experimental data in this work it is not possible to determine the exact mechanism, or at which point in time during testing the Ni particles leave their original position in the YSZ skeleton of the anode of the cell for the *YSZ-Hi* test. However it is clear that the nano-particles containing Ni and traces of sulfur are located in these Ni-lacking positions of the anode after test for the cell from the *YSZ-Hi* test. Even though the nano-particles contain Ni, the SEM images reveal that they do not constitute a percolating Ni network and therefore cannot act as new sites for the electrochemical reaction in the anode.

Cell overpotential was used as a test parameter to investigate the irreversible long-term performance loss due to H_2S poisoning. Based on the results reported here we find that the observed long-term irreversible degradation is triggered by the *combination of continued sulfur exposure and sufficiently high local oxygen potential (pO_2) in the anode structure*, particularly close to the electrolyte. In line with this, and based on long-term test for cells with Ni/YSZ and Ni/ScYSZ

based anodes,[11] we further hypothesize that the reported increased tolerance toward sulfur for Sc-doped Ni-zirconia based anodes compared to Ni/YSZ based anodes is also closely related to the local pO_2 in the anode structure, but the critical pO_2 necessary to initiate the observed irreversible long-term degradation is not necessarily identical for Sc-doped Ni-zirconia anodes compared to Ni/YSZ anodes.

Conclusions

From the results presented here it can be concluded that:

- At 850°C and a $CH_4/H_2O/H_2$ fuel it is possible to obtain (after the initial and reversible performance loss) very stable cell performance for both Ni/YSZ-based and Ni/ScYSZ-based cells i.e. cells with and without scandia-doping of the zirconia during 500 h addition of 2 ppm H_2S at 1 A/cm^2.[5,11]
- At higher cell overpotential (by increasing current density, but keeping the same fuel utilization) both Ni/YSZ-based and Ni/ScYSZ-based cells can be forced into a regime where the initial and reversible degradation due to the addition of 2 ppm H_2S is followed by an almost linear and irreversible degradation of the anode.
- Analyzes of electrochemical impedance spectra (IS) collected during galvanostatic testing for two Ni/YSZ-YSZ-LSM/YSZ-based cells show that for the low overpotential test (*YSZ-Low*) basically only $R_{Ni\text{-}TPB}$ is affected (reversibly) by H_2S poisoning and only in the initial stages. In contrast, significant irreversible increase in the high frequency part of the IS (ohmic resistance and ionic conductivity in the anode) was observed for the high overpotential test upon prolonged H_2S exposure (*YSZ-Hi*).
- The results from the *non-sulfur high overpotential* (*YSZ-no-S*) test in this work and previously reported test with similar cells with no H_2S addition for a Ni/YSZ-based cell suggest that the irreversible long-term degradation for the high overpotential H_2S-poisoning test (YSZ-*Hi*) is closely linked to the sulfur addition.
- The overpotential, rather than the current density or materials chemistry (since both YSZ and ScYSZ based anodes were tested), was found to be the key parameter for whether or not a given H_2S-exposure led to long-term irreversible degradation of the Ni-Zirconia based SOFC anodes.
- Post mortem analyzes by SEM shows that the cell from sulfur test with *low cell overpotential* (*YSZ-Low*) test and the cell from the *non-sulfur high overpotential* (*YSZ-no-S*) test both have satisfying percolating Ni network and porosities as expected when compared with a non-long-term tested cell.
- Post mortem analyzes by SEM shows that the cell from the sulfur test with *high cell overpotential* (*YSZ-Hi*) has a significant lower phase *fraction* and *number* of percolating Ni particles in the few microns of the anode closest to the electrolyte. Furthermore, this anode has an increased phase *fraction* of porosity in this same region of the anode but similar *number* of pores when compared to other tested cells.
- Nano-sized particles containing Ni and traces of sulfur can be found at the borders of the large pores in the innermost 2–4 μm of the anode from the heavily degraded and not fully recovered cell from the test with sulfur and high cell overpotential (*YSZ-Hi*).

Acknowledgment

Colleagues at DTU Energy Conversion are greatly acknowledged for technical assistance and fruitful discussions; especially H. Henriksen, M. Davodi, K. Brodersen, research Professor M. Mogensen and Dr C. Graves. Furthermore the authors acknowledge the financial supported from the project "Towards Smart Grid Ready SOFC", Energinet.dk project no. 2012–1–10747.

References

1. K. Haga, S. Adachi, Y. Shiratori, K. Itoh, and K. Sasaki, *Solid State Ionics*, **179**, 1427 (2008).
2. A. Hagen, *J. Electrochem. Soc.*, **160**, F111 (2013).
3. H. Kishimoto, T. Horita, K. Yamaji, M. E. Brito, Y. Xiong, and H. Yokokawa, *J. Electrochem. Soc.*, **157**, B802 (2010).
4. S. Zha, Z. Cheng, and M. Liu, *J. Electrochem. Soc.*, **154**, B201 (2007).
5. A. Hagen, J. F. B. Rasmussen, and K. Thydén, *J. Power Sources*, **196**, 7271 (2011).
6. K. Sasaki, K. Haga, T. Yoshizumi, D. Minematsu, E. Yuki, R. Liu, C. Uryu, T. Oshima, T. Ogura, Y. Shiratori, K. Ito, M. Koyama, and K. Yokomoto, *J. Power Sources*, **196**, 9130 (2011).
7. K. Sasaki, K. Susuki, A. Iyoshi, M. Uchimura, N. Imamura, H. Kusaba, Y. Teraoka, H. Fuchino, K. Tsujimoto, Y. Uchida, and N. Jingo, *J. Electrochem. Soc.*, **153**, A2023 (2006).
8. Z. Cheng, J. Wang, Y. Choi, L. Yang, M. C. Lin, and M. Liu, *Energy Enviro. Sci.*, **11**, 4389 (2011).
9. J. F. B. Rasmussen and A. Hagen, *J. Power Sources*, **191**, 534 (2009).
10. T. Yoshizumi, S. Taniguchi, Y. Shiratori, and K. Sasaki, *J. Electrochem. Soc.*, **159**, F693 (2012).
11. A. Hauch, A. Hagen, J. Hjelm, and T. Ramos, *ECS Transactions*, **57**(1), 615 (2013).
12. P. H. Larsen, C. Bagger, S. Linderoth, M. Mogensen, S. Primdahl, M. J. Jorgensen, P. V. Hendriksen, B. Kindl, N. Bonanos, F. W. Poulsen, and K. A. Maegaard, in *SOFC-VII*, H. Yokokawa and S. Singhal, Editors, PV2001-16, p. 28, The Electrochemical Society Proceeding Series, Pennington NJ (2001).
13. A. Hagen, R. Barfod, P. V. Hendriksen, Y. L. Liu, and S. Ramousse, *J. Electrochem. Soc.*, **153**, A1165 (2006).
14. A. Hauch, S. D. Ebbesen, S. H. Jensen, and M. Mogensen, *J. Electrochem. Soc.*, **155**, B1184 (2008).
15. S. Ramousse, M. Menon, K. Brodersen, J. Knudsen, U. Rahbek, and P. H. Larsen, *ECS Trans.*, **7**(1), 317 (2007).
16. C. Bagger, in *Fuel Cell Seminar*, p. 241, C. E. Pax, Editor (1992).
17. P. H. Larsen and K. Brodersen, patent, US2008124602-A1; JP2008130568-A; EP1930974-A1; CN101242003-A; CA2611362-A1; KR2008047282-A; KR966845-B1 (2008).
18. A. Hauch, C. Birkl, K. Brodersen, and P. S. Jørgensen, *Proceedings - 10th European Solid Oxide Fuel Cell Forum*, **Chapter 8**, 62 (2012).
19. M. Jørgensen and M. Mogensen, *J. Electrochem. Soc.*, **148**, A433 (2001).
20. J. Hjelm, M. Søgaard, R. Knibbe, A. Hagen, and M. Mogensen, *ECS Trans.*, **13**(26), 285 (2008).
21. A. Hauch, S. H. Jensen, M. Mogensen, and S. Ramousse, *J. Electrochem. Soc.*, **153**, A1741 (2006).
22. M. Mogensen and P. V. Hendriksen, in *High Temperature Solid Oxide Fuel Cells - Fundamentals, Design and Applications*, S. C. Singhal and K. Kendall, Editors, p. 261, Elsevier, London (2003).
23. J. F. B. Rasmussen and A. Hagen, *Fuel Cells*, **10**, 1135 (2010).
24. R. Barfod, M. Mogensen, T. Klemensø, A. Hagen, Y.-L. Liu, and P. V. Hendriksen, *J. Electrochem. Soc.*, **154**, B371 (2007).
25. A. Kromp, A. Leonide, A. Weber, and E. Ivers-Tiffee, *J. Electrochem. Soc.*, **158**, B980 (2011).
26. V. Sonn, A. Leonide, and E. Ivers-Tiffee, *J. Electrochem. Soc.*, **155**, B675 (2008).
27. T. Ramos, K. Thydén, and M. Mogensen, *ECS Trans.*, **28**(11), 123 (2010).
28. J. Nielsen, T. Jacobsen, and M. Wandel, *Electrochim. Acta*, **56**, 7963 (2011).
29. J. Nielsen, T. Klemensø, and P. Blennow, *J. Power Sources*, **219**, 305 (2012).
30. J. Nielsen and J. Hjelm, *Electrochim. Acta*, **115**, 31 (2014).
31. D. Johnson, Zview 2.8, Schribner Associates, Inc., USA (2003).
32. C. Graves, Ravdav ver0.9.5.1, Dept. of Energy Conversion and Storage, Technical University of Denmark (2012).
33. K. Thydén, Y. Liu, and J. B. Bilde-Sørensen, *Solid State Ionics*, **178**, 1984 (2008).
34. A. Tsoga, A. Naoumidis, and P. Nikolopoulos, *Acta Mater.*, **44**, 3679 (1996).
35. Z. Zeng, M. E. Bjorketun, S. Ebbesen, M. B. Mogensen, and J. Rossmeisl, *Phys. Chem. Chem. Phys.*, **15**, 6769 (2013).
36. A. Hauch, P. S. Jørgensen, K. Brodersen, and M. Mogensen, *J. Power Sources*, **196**, 8931 (2011).
37. C. Birkl, "Effect of anode sintering temperature on microstructure and performance of multilayer tape cast SOFC", MSc Thesis, Technical University of Denmark, Denmark (2012).
38. S. C. Singhal and K. Kendall, *High Temperature Solid Oxide Fuel Cells. Fundamentals, Design, and Applications*, Elsevier Ltd, Oxford, UK (2003).
39. Y. L. Liu, S. Primdahl, and M. Mogensen, *Solid State Ionics*, **161**, 1 (2003).
40. A. Hauch, S. H. Jensen, M. Mogensen, and J. B. Bilde-Sørensen, *J. Electrochem. Soc.*, **154**, A619 (2007).
41. A. Guebner, in *SOFC-V*, U. Stimming, S. C. Singhal, H. Takagi, and A. Leming Editors, PV97-40, p. 844, The Electrochemical Society Proceeding Series, Pennington NJ (1997).
42. A. Hauch, "*Solid oxide electrolysis cells - Performance and durability*", PhD Thesis, Risø National Laboratory, Technical University of Denmark, Roskilde, Denmark (2007).
43. L. Holzer, B. Muench, B. Iwanschitz, M. Cantoni, T. Hocker, and T. Graule, *J. Power Sources*, **196**, 7076 (2011).
44. A. Faes, A. Hessler-Wyser, D. Presvytes, C. G. Vayenas, and J. Van Herle, *Fuel Cells*, **9**, 841 (2009).
45. R. Knibbe, S. D. Ebbesen, A. Hauch, J. Hjelm, and M. Mogensen, *Green*, **1**, 141 (2011).
46. J. Wang and M. Liu, *Electrochem. Commun.*, **9**, 2212 (2007).
47. P. Lohsoontorn, D. J. L. Brett, and N. P. Brandon, *J. Power Sources*, **175**, 60 (2008).
48. R. Lohsoontorn, D. J. L. Brett, and N. P. Brandon, *J. Power Sources*, **183**, 232 (2008).
49. J. T. White, I. E. Reimanis, J. Tong, J. R. O'Brien, and A. Morrissey, *J. Am. Ceram. Soc.*, **95**, 4008 (2012).

50. H. Kishimoto, K. Yashiro, T. Shimonosono, M. E. Brito, K. Yamaji, T. Horita, H. Yokokawa, and J. Mizusaki, *Electrochim. Acta*, **82**, 263 (2012).
51. S. Linderoth, N. Bonanos, K. V. Jensen, and J. B. Bilde-Sørensen, *J. Am. Ceram. Soc.*, **84**, 2652 (2001).
52. M. Brown, S. Primdahl, and M. Mogensen, *J. Electrochem. Soc.*, **147**, 475 (2000).
53. K. Chen, X. Chen, Z. Lü, N. Ai, X. Huang, and W. Su, *Electrochim. Acta*, **53**, 7825 (2008).
54. S. Kavurucu Schubert, M. Kusnezoff, A. Michaelis, and S. I. Bredikhin, *J. Power Sources*, **217**, 364 (2012).
55. Y. M. Park, H. J. Lee, H. Y. Bae, J. S. Ahn, and H. Kim, *Int. J. Hydrogen Energy*, **37**, 4394 (2012).